CHAPTER 36

Localizing Cingulate Subregions-of-Interest in Magnetic Resonance Images Guided by Cytological Parcellations

Joseph O'Neill, Thomas L. Sobel, and Brent A. Vogt

Chapter contents

Understanding of the cytoarchitectural and functional subdivisions of cingulate cortex has greatly advanced in recent decades. Yet, use of the original Brodmann areas (BAs) delineated in his 1909 classic remains entrenched in human neuroimaging research. The same is true for his dichotomy of cingulate cortex into anterior and posterior divisions and this is mainly attributable to Talairach and Tournoux (1988). Their celebrated stereotaxic atlas of the human brain provides the Brodmann nomenclature most used to identify activity or structures in a standard space without reference to particular cytoarchitectures. What many investigators using this atlas do not realize is that, among other flaws, the single case in their atlas was never itself histologically analyzed. As no single imaging study has ever activated the entire BA24, the current trend is to apply numerous designations to cingulate regions and subregions, without specific justification, as the findings fail to corroborate Brodmann's original conceptualizations. This is particularly true of anterior cingulate cortex (ACC) as discussed in Chapter 1. Without specific justification from cytology and connections, recent studies have applied numerous designations to the anterior cortex such as rostral/caudal, dorsal/ventral, or superior/inferior. We still do not know the limits of any of these imaging designations because they refer to activation sites rather than to cytoarchitectural entities. What the cytoarchitecture is and what functional constructs account for the designation of these sites as unique cortical entities is not known. There is no neurocytology to define their boundaries and there is no clarity as to the connections that subserve any of these vague designations or assumed functions. Thus, there has been a slow drift away from the Brodmann model without an explicit understanding of what is being done and why, while implicitly continuing to use his two-region model.

There have been a few instances in which current cytological methodologies are used to define the structural and transmitter receptor organization of areas in standard coordinate systems (Zilles & Palomero-Gallagher, 2001; Vogt *et al.*, 2003, 2006). The importance of these efforts arises from their defining structurally unique entities such as has been pioneered in sensorimotor systems. Investigators of the human brain are in need of a method whereby findings in the neurobiology literature (neuron structure and immunohistochemistry, network connections, neuropathology) can be systematically translated into neuroimaging coordinates. The present chapter seeks to link the findings of cingulate neurobiology with those of human neuroimaging so that information generated in different academic research undertakings can be directly interrelated without introducing confusing new nomenclatures for each report of activity and structural imaging finding.

Cingulate Parcellations in Neuron-free, Structural Images

Many structural imaging studies have attempted to parcellate the cingulate cortex with macroanatomical landmarks including the vertical plane at the anterior commissure (VAC). Of course, there is no *a priori* reason to predict that the VAC links in any systematic way to cingulate cytoarchitecture or any cortical developmental process. Its value arises because it presents a small and easily identifiable medial surface landmark; hardly a profound rationale for its use in studying cingulate cortex. Moreover, the history of citing BAs was an early attempt to locate structural entities observed more than a century ago. This map, however, is very incomplete in terms of cingulate cortex and its application by Talairach and Tournoux (1988) is flawed on many accounts including a lack of postmortem histology. The practice of citing BAs to locate structural entities is becoming confused as investigators realize that Brodmann's partitioning has no functional significance (Chapter 1). Instead, there are now many studies that parcellate with sulci and vague references to Brodmann's original report with the underlying view that these concepts, in some unstated way, still have merit. This approach involves generating new adjectives for activations and structures and an emphasis is on parts of the cingulate gyrus rather than its entirety.

An example of a parcellation scheme based on neuron-free images in ACC is provided by McCormick *et al.* (2006). In this study, the paracingulate sulcus (pcgs) was renamed the 'major cingulate sulcus,' while the cingulate sulcus itself was renamed the 'minor cingulate sulcus.' The term 'paracingulate' used in the past is an excellent term because this sulcus lays adjacent ('para') to cingulate cortex and the cingulate sulcus of times past is also an excellent term because it is associated with the full length of the cingulate gyrus rather than just its rostral aspect in ACC. Certainly, the 'minor cingulate sulcus' is not minor in PCC and the 'major/minor' designations blur equivalent links to the monkey where the comparative cytoarchitecture of primates becomes a major concern (Chapter 3). Another new aspect of the McCormick *et al.* (2006) study is the designation for 'Dorsal ACC' which has been extended beyond its use by Bush *et al.* (2002) who pioneered its use. The latter authors applied it to cortex comprising areas 32′ and a24c′ as discussed in Chapter 12, while the 'new' 'Dorsal' 'ACC' encompasses part of ACC, all of midcingulate cortex (MCC), and some of dorsal PCC. Although it is claimed that the Dorsal ACC is a uniform functional region, there is so much evidence to the contrary that one will need to consult many of the chapters in this volume. Finally, there is some confusion regarding the corpus callosum. The genu is a division of

the corpus callosum and it is incorrect to designate two cortical regions ventral to the genu as 'subgenual' and 'subcallosal' because the genu is part of the corpus callosum in both instances. Thus, this study emphasizes a modern reworking of cingulate organization with human neuroimaging that generates more problems than it resolves.

There are many ways to avoid parcellating the brain with only neuron-free structural images but they require time consuming, independent methods to identify structural borders. These include receptor binding statistics (Chapter 2), correlated clusters of glucose metabolism (Chapter 1), cytoarchitecture (Chapter 3), or mapping-specific projections such as those from the amygdala and parietal cortex (Chapters 1 and 13). We spent a few decades re-evaluating the Brodmann scheme from cytological, connections, and functional perspectives and have generated a qualitatively different view of the organization of this cortex. Indeed, the integrative, neurobiological approach, and a focused research strategy with a rational nomenclature provide the means of moving past macroscopic methods. The method outlined below builds on the long tradition of cytoarchitectural analysis started for the human by C. and O. Vogt during the early part of the 19th century.

The Eight-Subregion Model

Over the past two decades, most investigators have become aware of the failure of Brodmann's anterior cingulate concept. There has never been a functional study to activate this entire region nor have connection or cytological studies observed this to be uniformly and selectively innervated by any cingulate afferent. In spite of these facts, the anterior cingulate concept of Brodmann remains unchanged and findings of human imaging research are pressed into this format according to the 'BA' designations generated by Talairach and Tournoux (1988). Many of the problems with this atlas center on the fact that Brodmann did not present the sulcal areas in his folded map of the cerebral cortex. One of the most consistent failures of the Talairach and Tournoux atlas in this regard is the localization of the retrosplenial areas on the posterior cingulate gyral surface rather than in the callosal sulcus (Vogt *et al*., 2001).

An alternative view has been systematically validated by many functional, connectional, and cytoarchitectural analyses over a period of three decades. Pivotal to this approach is the midcingulate concept first proposed for the rabbit and monkey brains (Vogt, 1993). The resulting four-region neurobiological model has been evaluated in rat (Vogt *et al*., 2004a,b), rabbit (Sikes *et al*., 2008), monkey (Vogt *et al*., 2005), and human (Vogt *et al*., 2004b) and will not be reviewed here. In the early part of the present decade, it became clear that even these four regions were not uniform entities and they were further subdivided (MCC: Vogt *et al*., 2003; PCC: Vogt *et al*., 2006) as also discussed in Chapters 1, 3, and 13. This process has resulted in eight subregions termed from rostral-to-caudal: (1) subgenual ACC; (2) pregenual ACC; (3) anterior MCC; (4) posterior MCC; (5) dorsal PCC; (6) ventral PCC; (7) dorsal retrosplenial cortex (dRSC); and (8) ventral RSC (vRSC). Each subregion is comprised further of areas and these areas of subareas. A few comments on using this nomenclature are needed because it is not always apparent how and why particular histological concepts are used. We will not consider the dichotomy of RSC in detail until imaging studies can routinely isolate this small region.

An *area* is a uniform cytoarchitectural entity and it is defined by the size, shape, and packing densities of neurons according to horizontally dispersed layers and vertically oriented clusters or aggregates of neurons. There may be short transitions between areas but they are usually less than a few hundred micrometers in length. Unfortunately, very few areas are cytologically uniform and none of Brodmann's areas were cytologically uniform. Thus, they are further divided into *subareas*. This was first detailed in the dorsal-to-ventral (z-) plane and characterized with the letters a–d in the monkey (Vogt *et al*., 1987). With the recent addition of the MCC, the use of the prime (e.g., area 24′) was adopted to distinguish MCC from the corresponding and adjacent ACC areas (e.g., area 24). As all areas have a number of subareas, we continue to refer to all cytologically uniform cortices as 'areas.'

A *region* is comprised of two or more adjoining and cytologically unique areas. These are usually oriented ventral-to-dorsal following the direction of cortical differentiation and presumably its development in the primate. As already noted, however, even the regions are heterogeneous in terms of their functions, connections, neuronal phenotypes, and laminar architecture; *subregions* attempt to capture these differences. A subregion is comprised of two or more cytologically unique areas within a region. Functional subregions may also be defined that bridge two or more anatomic subregions. For example, the spinal cord projections of the cingulate motor areas arise from neurons on the dorsal and ventral banks of the cingulate sulcus in MCC and PCC (Chapters 1 and 5). In another example, vocalization can be evoked by electrical stimulation in the ACC including parts of areas 24 and 32 in what is termed the cingulate vocalization subregion (Chapter 15). Figure 36.1 provides a summary of the four regions, eight subregions and various areas for ACC, MCC, PCC, and RSC.

This simple nomenclature allows navigation anywhere in the cingulate gyrus regardless of the topic or magnification. Here we provide simple rules by which all can agree to the application of the neurocytological

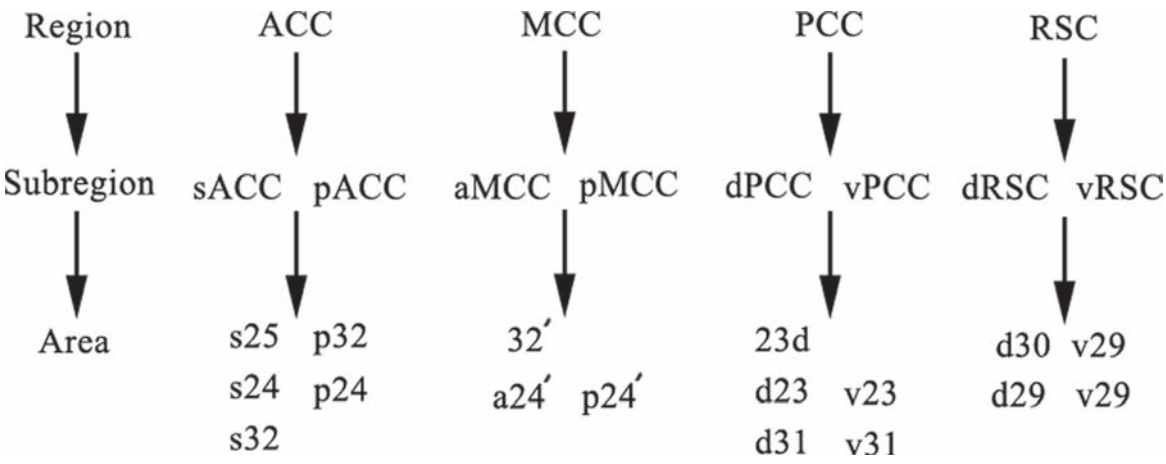

Fig. 36.1 Nomenclature of cingulate cortex in the form of a decision-tree beginning at the largest identifiable component which is the region, the subregions next and finally each cytoarchitectural area within a subregion. The subregion is the smallest unit that can usually be identified with current macroscopic imaging methods.

analysis to human structural images that have no cellular information. In practice, the need to identify these subregions-of-interest (SOIs) will frequently arise when only structural data are available or when these data are the most practical to use. There is intrinsic interest in measuring the sizes and shapes of cingulate subregions that is not confined to cases where corroborating histological and functional neuroimaging data are available. Furthermore, many functional imagers prefer to define cingulate subregions with independent anatomic criteria and then characterize their findings as occurring within one or more subregions rather than defining the cingulate subregions based on functional responses. Also, most areas/subareas, including the divisions of RSC, are beyond the resolution of current imaging and their consistent identification awaits further progress in improving resolution as well as the more widespread availability of existing technologies (e.g., ultra-high-field magnetic resonance imaging [MRI]). Finally, due to the substantial variability in the location, orientation, and segmentation of the various sulci in cingulate cortex, all but the callosal sulcus cannot be used to define the limits of areas, regions, or subregions. As the borders of subregions have been defined histologically, we use a system to first identify these borders and allow the variability in sulci to be expressed within the subregional unit such that the sulcal variability contributes little to the voluming method.

High-resolution MRI at 1–4 T field strength is currently the preferred neuroimaging modality for anatomical parcellations of the brain. Some analyses identify cingulate structures in 'native space;' i.e., a subject's MRI volume acquired in its unaltered dimensions apart from non-distorting reslices and rigid rotations and translations in what is called a 'region-of-interest' (ROI) approach. Other analyses use standard atlas spaces such as Talairach and Tournoux (1988) or the MNI305 atlas (Collins, 1994; Evans *et al*., 1993), since supplanted by the ICBM152 space (Mazziotta *et al*., 1995). Use of atlas space entails transformation or 'warping' of the single-subject brain from its native space into the corresponding atlas space. Warping distorts the MRI volume, but most researchers deem this an acceptable disadvantage of the use of atlas space. Although the eight-subregion model is the most comprehensive and integrative systematization of information on cingulate cortex available and offers a rational simplification of the currently reigning chaos in cingulate anatomic nomenclature (see Chapter 1 'Recent Imaging Approaches to Cingulate Nomenclature'), a substantial obstacle to the adoption of the eight-subregion model as a standard in neuroscience is the fact that there currently exists no MRI-based protocol for a comprehensive parcellation of the human cingulate cortex into all eight subregions; nor are the subregions yet properly localized in Talairach or ICBM152 space. Here we attempt to remedy these deficiencies, keeping in mind the limitations of a purely macroanatomic approach, by providing instructions for drawing the subregions (apart from RSC) in Talairach and ICBM152 atlas spaces based on a histologically assessed template case GPC. Reports based on a larger sample of histological cases are provided elsewhere (Vogt *et al*., 2003, 2006).

A Template Case with Rigorous Histology

Case GPC

The histologically analyzed medial surface used throughout this volume is from Case GPC; an 80-year-old,

right-handed, white male who died of pneumonia and retroperitoneal hemorrhage. There was no clinical history of neurologic or psychiatric disorders and no reports of cognitive deficits before death according to conversations with family members and medical records. The brain weight was 1360 g at post-mortem and the medial fillet from each hemisphere was 1.75 cm thick to include the full depths of medial surface sulci. The fillets were post-fixed in paraformaldehyde, immersed in a graded series of sucrose solutions, stored in 30% sucrose and sodium azide and digitally photographed. Coronal blocks were made including a wedge block for reorienting sections as shown in Figure 36.2A. The brain was photographed again and the blocks cut into 10 series of 50-µm-thick sections. A series was stained for thionin, neuron-specific nuclear binding protein, non-phosphorylated intermediate neurofilaments (SMI32 antibody), and calretinin. Three sections per block were also reacted for amyloid-β42 peptide and they were negative for this protein. There are approximately 4,000 sections available from this case and we have spent 9 years in detailed studies of it. Further methodological details are provided elsewhere (Vogt *et al.*, 2003, 2006) and an extensive series of photographs at specific points in GPC are shown throughout Chapter 3.

The goal of histological sectioning is to cut sections that are optimally oriented parallel to the apical dendrites of large pyramidal neurons. All effort is made to avoid oblique sections such that the superficial layers are in register with their counterparts in the deep layers to assure that the aligned layers are part of the same areas. This problem is not encountered in structural images where neurons and dendrites are not available for analysis. As the cingulate and paracingulate gyri are almost constantly reorienting around the genu of the corpus callosum, we use a midcingulate wedge block (W, Fig. 36.2A) to reorient the blocks to an approximately parallel plane of section in ACC and PCC. In some instances, we cut horizontal blocks rostral to the genu and caudal to the splenium to achieve ideal sections at these two sites.

Landmarks and orientation

The problem at hand is not how to generate the easiest slicing and SOI determination from images readily available with current software packages. The problem is one of neurobiology: how do we co-register information best achieved with histological sections with that from structural neuroimaging such that both classes of qualitatively unique information can be joined in a consistent manner? Our approach is to match high-resolution structural MRI volumes of the cingulate cortex in a cerebral hemisphere to a histologically verified specimen. We make our principal comparisons using parasagittal sections of the test subject's MRI and the flat map of the histologically verified specimen. Thereby, the MRI has been pre-transformed into Talairach or ICBM152 space and the flat map has been reoriented (but not yet rescaled) into the Talairach coordinate system (which is used, with different scaling, for both Talairach and ICBM152 atlas spaces). As our

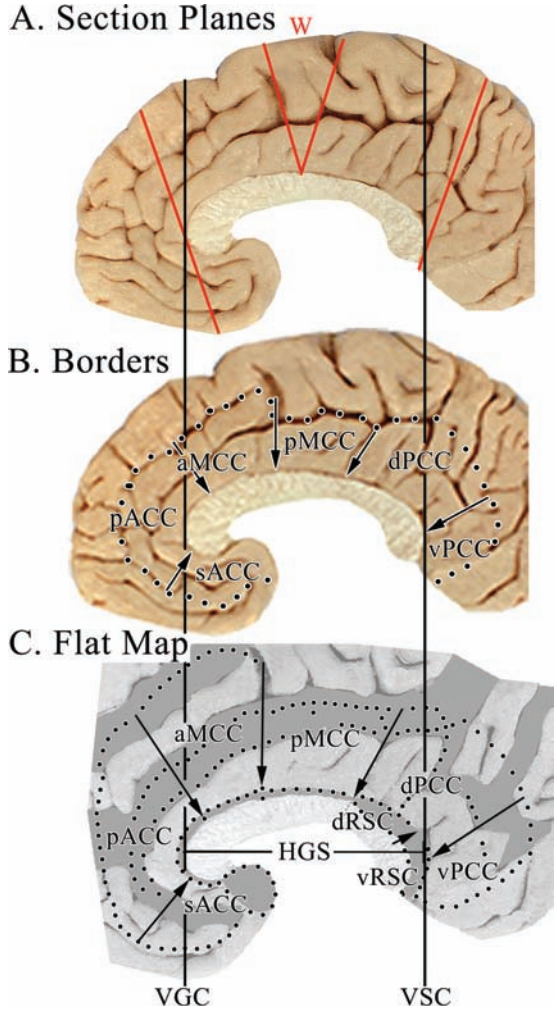

Fig. 36.2 Subregions in case GPC. Each image is oriented in the horizontal plane along the rostral edge of the genu and caudal edge of the splenium of the corpus callosum (HGS; C.). The two cingulate verticals (perpendicular to HGS) are indicated at the genu (VGC) and splenium (VSC). Notice that demonstration of RSC in C. required deforming the splenium such that co-registration of the VSC in the flat map is to the caudal edge of RSC. In A., the 'W' is the wedge block and planes of section for histological analysis are shown in red. Two types of information are derived from this case: the borders and external limits of cingulate cortex are shown in the native cortex images (B.), while the composition of the sulcal cortex is provided in the flat map (C.). The flattening procedure is primarily in the dorsal direction such that the corpus callosum can be used to orient and scale the case. Flattening in rostral and caudal directions is performed rostral and caudal to the VGC and VSC, respectively.

flat map, we use the right hemisphere of case GPC in Figure 36.2.

Cingulocentric landmarks, including features of the corpus callosum, are used because there is no reason to expect that development of the anterior commissure or other commonly used landmarks for whole brain analysis are linked to the structure, connections, or functions of the cingulate gyrus. There may be interesting correlations between the VAC and functional activation sites but there is no reason to expect a causal relationship from a developmental perspective. The corpus callosum, in contrast, does develop in close proximity to the cingulate gyrus; hence its anatomic features are a more likely guide to the locations of cingulate SOIs. Thus, the medial surface is aligned with the corpus callosum (i.e., callosal sulcus) which is oriented on a horizontal plane through the rostral tip of the genu and caudal tip of the splenium of the corpus callosum (HGS) as shown in Figure 36.2C.

Comments on Sulcal Variations in Relation to SOIs

The issue of sulcal variation throughout the cerebral cortex (Ono *et al.*, 1990) as well in cingulate cortex (Vogt *et al.*, 1995, 2004b) is well known and will not be restated. Figure 36.3 provides some examples of variability noted in MRI cases including both hemispheres for Case #3. The two main patterns of sulci are the single cingulate sulcus (cgs) and the double parallel pattern of cgs and pcgs. The latter pattern refers to cases where both sulci are relatively well defined (continuous or large segments and little collateral branching; e.g., Case #3 right hemisphere). The single cgs pattern refers to cases where only the cgs is well defined and examples are Cases #1, Case #3 left hemisphere, and Case #4. These terms can be misconstrued, however. The fact that a hemisphere exhibits the single cgs pattern does mean that it does not have a pcgs. The pcgs is usually present, but can be difficult to trace in some instances because it is broken into multiple segments along its course. The segments can be oriented in a vertical or horizontal direction. In fact, there are few instances where segments of the pcgs cannot be identified. Thus, there is never a state in which there is no pcgs and studies that propose to identify cases in which the pcgs is absent usually overlook fragments of this sulcus. Certainly, the implication of such work that an area 32′ is not present is spurious. Finally, the distinction between the cgs and pcgs can be difficult around the genu of the corpus callosum and Case #2 is an example of a highly anastomized sulcal pattern in ACC (circled).

Variations in sulcal patterns make it difficult to assign cingulate areas based on gross anatomy. Where there are clear double parallel sulci (Case #3 right), the cgs and external cingulate gyrus are easily located. When the latter is clear, it is relatively straightforward to

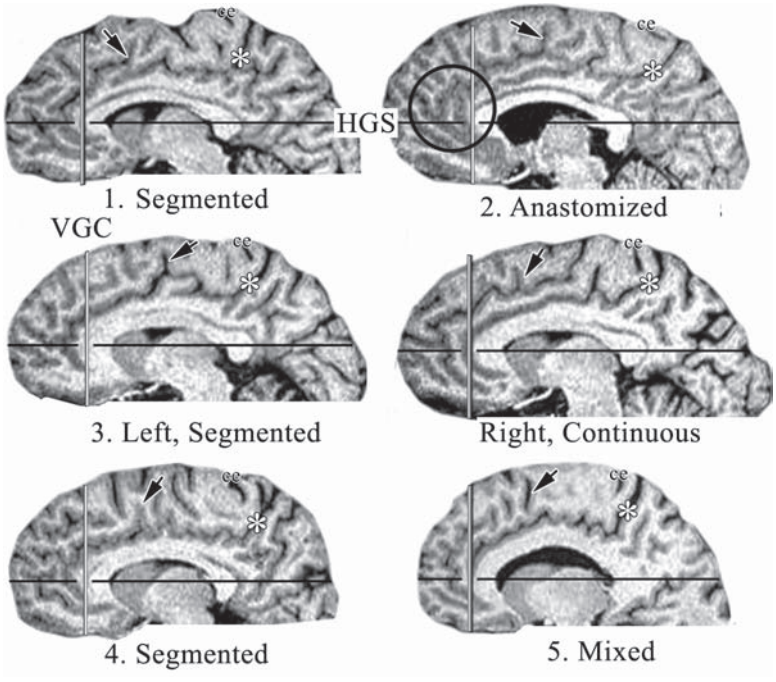

Fig. 36.3 Medial surfaces at x = 5 mm for a sample of cases in MRI. The greatest variability is in the structure of the pcgs which is segmented, continuous, anastomized or mixed. The brains were oriented parallel to the horizontal plane at the genu and splenium (HGS) and the vertical plane at the genu (VGC) is shown. The marginal ramus (mr) of the cgs is marked with an asterisk and the medial edge of the central sulcus (ce) and the dorsal ramus of either the pcgs or cgs (arrowheads) are marked.

locate areas 32 and 32′. When the pcgs is disordered as in Case #2, no secure statement can be made about the location of area 32. This point once again emphasizes that it is virtually impossible to localize specific cingulate areas in a large population of cases with MRI. For this reason, we emphasize localizing SOIs rather than areas.

The emphasis on SOI localizations allows for intrasubregional variation of sulci without reaching too far to define single areas that are impossible in neuron-free structural images. The SOI localizations provide a secure basis for definition with the co-registered flat map in spite of sulcal variation. Thus, comparison of volume rendered SOI values should be relatively comparable in spite of sulcal variation therein and this view will be further analyzed below.

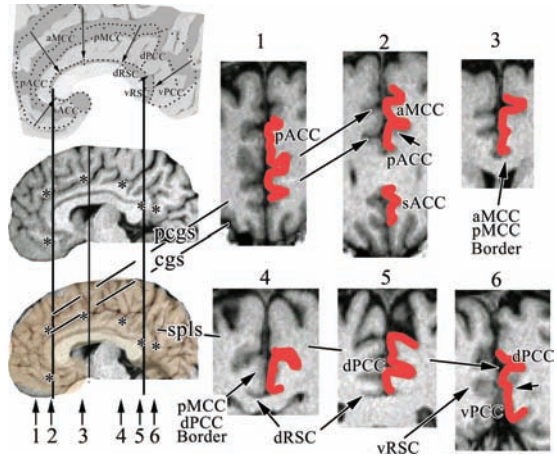

Fig. 36.4 Identification of the subregions in Talairach space involves guidance from the co-registered flat map overlay at 50% opacity. The outer boundaries of anterior cingulate cortex and midcingulate cortex (MCC) are determined by the pcgs. Notice that part of the pcgs in native space is actually removed from anterior midcingulate cortex (aMCC) during the normalization procedure (circle in Fig. 36.6B.) The edges of posterior cingulate cortex are impossible to determine in a specific manner, however, a few reasonable 'rules' are provided in the text.

Identifying Subregion Borders in the Rostral-Caudal (y-) Axis

The mean boundaries in 6–8 cases have been reported for MCC (Vogt *et al*., 2003) and PCC (Vogt *et al*., 2006) and these values are expressed as distances in millimeter from VAC based on cytoarchitecturally identified areas after mutual alignment in Talairach space. When these values are calculated in Talairach rather than native space, there is surprisingly little variation among the boundaries. The borders between each pair of SOIs are marked with long arrows on the flat map in Figure 36.2 (see also Chapter 3/Fig. 3.17). As Case GPC is one of the cases in these two series, it plays a significant role in determining the average borders and actually reflects the average border location quite well.

It is important to note that structural imaging studies that require cortical flattening generally begin with the question of aligning and standardizing the entire brain. This approach generates distortions throughout the brain, including some volumetric, three-dimensional changes in cingulate cortex that are not associated with cingulate cortex itself but with distortions generated from the lateral surface. An alternative, cingulocentric approach is discussed in Chapter 3. It begins with a two-dimensional image of the medial surface rather than the three-dimensional brain and uses unique features of this surface for fiducials and distortions when flattening. Thus, flattening distortions can be limited to only one dimension without reference to the lateral surface. The map from Figure 3.17 was flattened from the corpus callosum in one direction—dorsally—to preserve relationships with the callosal sulcus. Notice that the splenium was rotated ventrally to show the RSC and co-registration to the splenium requires using the caudal edge of RSC where the caudal edge of the splenium actually resides (see also Fig. 36.2). Further flattening in the rostral and caudal directions associated with the pcgs and splenial sulci (spls) extends the map rostrally and caudally beyond the corpus callosum but does not disrupt the location of each border dorsal to the corpus callosum. Thus, this cingulocentric orientation and landmark strategy produces less overall distortion in the cingulate gyrus, more precise designation of SOI borders guided by histological analyses, and the capability of co-registration to structural images.

The flat map outline for co-registration to individual cases in native or Talairach space is available from the web site for Cingulum Neurosciences Institute: www.cingulumneurosciences.org

The methods used here are best applied on high-resolution structural MRI, e.g., Siemens or GE MPRAGE, or SPGR commercial product sequences. Voxel dimensions of 1.5 mm or less on a side, ideally 1 mm or less, are preferred. Use of isotropic, for example, 1 mm^3 voxels as acquired or reconstructed is helpful, though not essential. Investigators may co-register and average multiple MRI scans from the same subject to enhance signal-to-noise ratio. Our sample volumes were post-processed using the MIPAV medical image processing software package developed at NIH (http://mipav.cit.nih.gov/) and the Display program of the LONI tools software suite (http://www.loni.ucla.edu/Software/), which is drawn from the Minctools software suite (http://packages.bic.mni.mcgill.ca/). Other packages, for example, FSL, Medx, and BRAINS2, may also serve. Specific instructions follow.

Prior to parcellation, the brain is oriented along the AC–PC line and transformed into Talairach or ICBM152 space. For simplicity, in the following, we will merely refer to Talairach space, though similar operations are used for ICBM152. Most of the work is done in sagittal view with occasional reference to the coronal view. Select a hemisphere (each must be processed separately) and, with the brain in sagittal view, find the midline slice. Then scroll to a slice ~5 mm lateral to the midline where there is a good view of the medial surface of cingulate cortex. The histological flat map is also a parasagittal section at 5 mm lateral. As described in Vogt *et al*. (2003, 2006), it has been aligned to the Talairach coordinate system, but has not yet been *rescaled* to the dimensions of Talairach space. The latter is intentional. As mentioned, each individual brain undergoes its own degree of distortion during the transition from native to Talairach space. Even after the transition, different individual brains in Talairach space are *not* morphologically identical. As we wish to use the flat map from one representative post-mortem subject to identify the cingulate SOIs of multiple subjects' MRIs, we rescale the flat map not to the standard Talairach brain, but to each individual subject's brain in Talairach space. This is done furthermore using a *cingulocentric* approach as described above. Take a screenshot of the parasagittal section and export it (as *.jpeg or other common picture format) to Adobe Photoshop or a similar image-processing package and import the flat map into Photoshop. Adjust the flat map to 50% opacity and overlap it onto the MRI section. Investigators interested in this method may wish to streamline the technique to by-pass the excursion to Photoshop and work directly in MIPAV or Display.

In Photoshop, shift and rotate the flat map as required until its VGS and vertical plane at the splenium of the corpus callosum (VSC) are parallel to those of the MRI; the HGS of the flat map, and of the MRI should also be parallel. This represents an adjustment to the original alignment of the flat map to the Talairach coordinate system. Now change the scale of the flat map (expansion or contraction) until the vertical hash mark at the rostral end of the horizontal HGS bar is tangent to the rostral extreme of the genu of the corpus callosum. The anterior boundary of the vRSC and dRSC should be aligned with the splenium of the corpus callosum, leaving the vertical hash mark at the caudal end of the HGS bar slightly posterior to the splenium (compare Fig. 36.2C); remember the splenium was rotated ventral in the flat map. This operation replaces the rescaling or warping step of the conventional Talairach transform. The rescaling is cingulocentric because it uses the corpus callosum, a structure that co-develops with the cingulate gyrus, to set the scale. Then make what adjustments are possible (e.g., slight vertical shifts and rotations) to fit the dotted inner boundaries of the flat map along the external margins of the corpus callosum and the internal margin of the subgenual anterior cingulate cortex (sACC) (Fig. 36.2C). The long arrows on the flat map now provide the rostral–caudal boundaries between adjacent cingulate SOIs on the MRI.

Once the flat map is aligned, zoom it to match the size of the sagittal MRI in MIPAV or Display and position the two images side-by-side. The inter-SOI boundaries can be transferred to the test subject's MRI as follows. Measure the angle with respect to the vertical (VGC, VSC, or VAC) of each long arrow and its starting point at the callosal sulcus. Using the drawing tools of MIPAV or Display, draw a straight line segment with outward trajectory on the MRI with the same angle and starting point as the corresponding long arrow on the histological control flat map. Do this for each of the boundary lines. Alternatively, for each inter-SOI boundary identify a pair of landmarks on the sagittal MRI and use these two points to draw the boundary line. Note that, due to our limited MRI spatial resolution ($1 \times 1 \times 1$ mm^3), we opted not to draw the vRSC and dRSC, but merely subsumed these into the ventral posterior cingulate cortex (vPCC) and dorsal posterior cingulate cortex (dPCC), respectively. Other investigators, particularly those with higher resolution, may attempt to volume the vRSC and dRSC using the flat map but these subregions are small so this is difficult. Once the inter-SOI boundaries for sACC/pregenual anterior cingulate cortex (pACC), pACC/aMCC, aMCC/posterior midcingulate cortex (pMCC), pMCC/dPCC, and dPCC/vPCC have been drawn, the inner boundaries of each of these SOIs may be drawn along the cas. The next, and more difficult, task is to identify the outer SOI boundaries.

Evaluating the External Subregion Limits

The 50% opacity flat map provides the subregion borders around the cas but cannot be used to identify the outer edges of cingulate cortex. When the pcgs is continuous or segmented, as for the case in Figure 36.5, determining the depth of this sulcus is straightforward. The problem arises in PCC for all cases as this border cannot be extrapolated uniformly from macroanatomy in this region. It is generally true that the border of cingulate and parietal cortices approximates one-third the distance dorsal to the knee of the marginal ramus (mr) as shown in Figure 36.5. The middle of the spls (usually forms an 'H' and this refers to the horizontal line in the 'H') should be embodied in the PCC but PCC does not encompass all dorsal branches of the spls as they often extend into parietal cortex. This extension is shown in the figure as well. The final extension of the

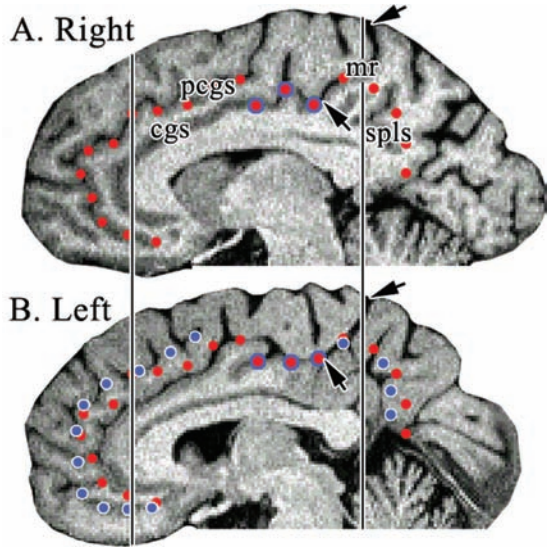

Fig. 36.5 This case is in native space and was selected because of the clear and continuous pcgs in the right hemisphere that matches that of case GPC. In this instance, the depth of the pcgs is easily determined and, even though segmented, can be determined in the left hemisphere as well. The blue-stroked red dots are points that are almost the same in both hemispheres. The arrowheads show the limits of the marginal ramus (mr) in both hemispheres that are used to gauge the starting points for the border of PCC. The red dots from the right hemisphere were transferred to the left for comparison.

outer edge of PCC is continued around to the splenium at approximately 50% of the mr distance. Without cytoarchitecture for each case, this will always be a weak identification.

Other views of the location of borders and edges of the SOIs are provided in Figure 36.6 and in the coronal sections of Figure 36.4. The insets depicting the six coronal sections have cingulate cortex highlighted in red with borders assessed using both the flat map and external sulci. As discussed, the propensity of the pcgs to meander, to split into segments, and to merge with the underlying cgs makes this boundary challenging to assign in some hemispheres. Drawing the pcgs boundary in non-obvious cases requires some experience. It is basically a process of identifying and linking the horizontal and vertical segments of the pcgs. The cases illustrated in this chapter should serve as a guide as we have intentionally selected both 'easy' and 'difficult' cases to provide an impression of the range of variability in the normal adult human brain. Note also that in all cases the outer/dorsal bank of the pcgs is assigned to extra-cingulate tissue. Finally, the pcgs outer boundary is not continued posterior to the aMCC; starting with the pMCC, the outer boundary drops down to the cgs. This latter criterion is based on observations in many cases, however, there are rare instances in which the pcgs extends throughout pMCC and this is currently assumed to contain premotor rather than cingulate cortex.

Voluming the Subregions

Once the interregional, inner, and outer SOI boundaries have been drawn on the sagittal MRI slice at ~3 mm lateral to midline, the individual SOIs can be volumed, that is, drawn in all three dimensions. The voluming can be done in sagittal view, with occasional aid of the coronal view. To volume the SOIs, scroll medially and laterally through the MRI slices one-by-one. Copy and paste the SOI boundaries from each successive slice onto the next slice. Then adjust the boundaries to match the anatomy on the slice. Voluming stops just after the sulcal fundi are reached, i.e., when the cortex transitions into white matter. Note that this transition can occur on different sagittal slices for the different SOIs and on different slices for the cgs and pcgs within an SOI. Also, as mentioned, the two cerebral hemispheres must be volumed separately. The SOI volume is obtained by summing the areas across all the slices and multiplying by the slice thickness. Figure 36.4 illustrates the method for a test case. In this figure, cingulate subregions have been painstakingly outlined to include only cortex (i.e., gray matter). Alternatively, saving time and effort, one may include subcortical white matter and sulcal cerebrospinal fluid (CSF) along with cortex in the SOI parcellation. When this is done gray matter, white matter, and CSF portions of the subregion may later be segregated away by overlapping the SOI volume with whole-brain gray-matter, white-matter, or CSF masks generated by semi-automated MRI tissue-segmentation (e.g., Blanton *et al.* 2001; Shattuck *et al.* 2001). The complete algorithm for parcellating the cingulate into SOIs according to the Eight-Subregion Model is summarized in Table 36.1.

Applying the Protocol to the Five Test Cases

To test the method across a wide range of normal cingulate anatomy, we processed the five subjects (six hemispheres) of Figure 36.3 using the above protocol. As mentioned, some of these cases were chosen specifically because they represented difficult cases in terms of identifying the pcgs. All were healthy subjects who had passed screening for neurologic, psychiatric, and major medical disorders. All subjects' brain MRIs were judged as normal by a radiologist. The subjects comprised three men and two women, ranging 22–48 years in age (Table 36.2).

Figure 36.7 shows the parcellations of the six hemispheres achieved with the method in ICBM152 space.

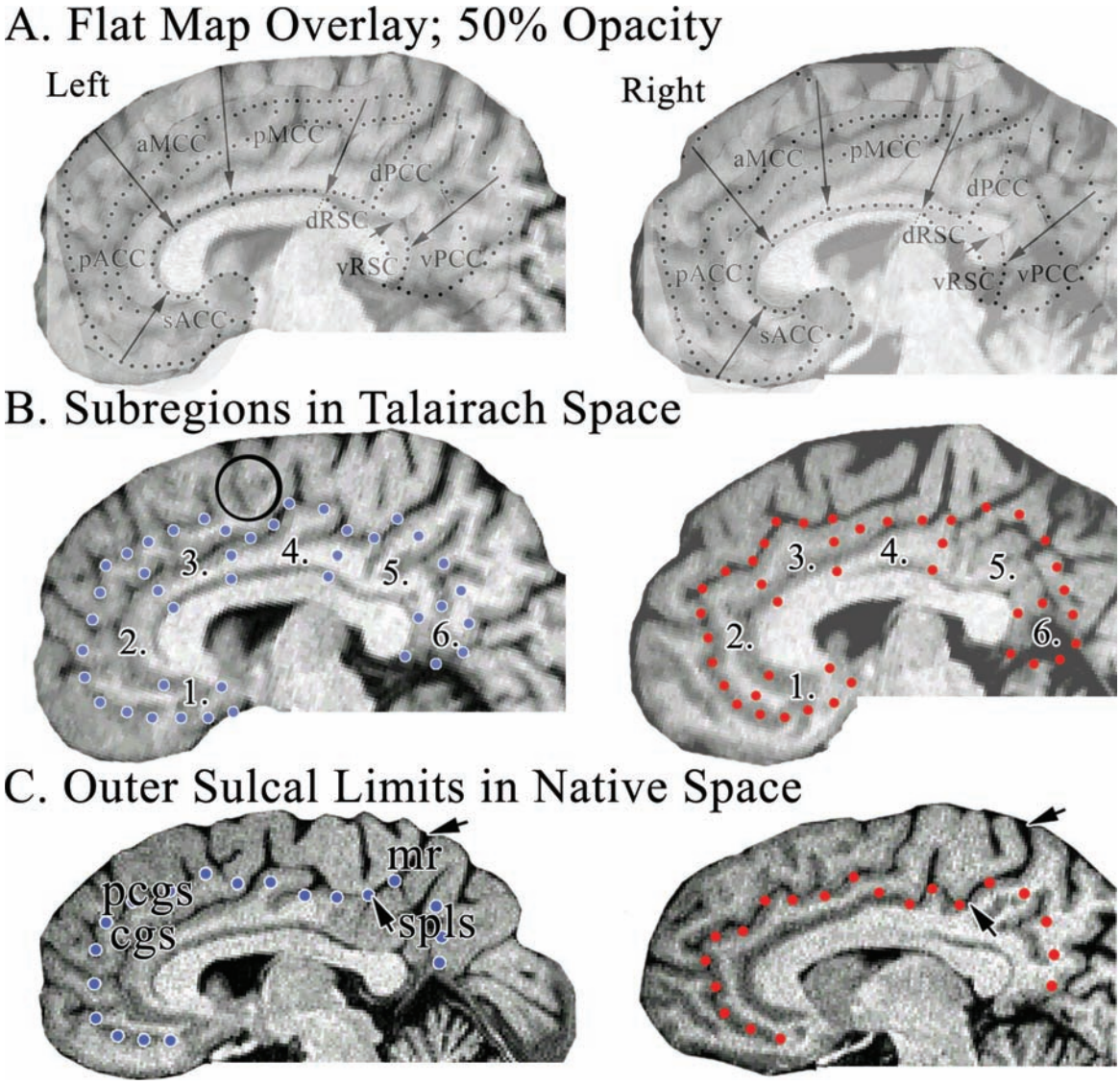

Fig. 36.6 T1-weighted whole-brain MRI sections ~5 mm lateral to sagittal midline in left and right cerebral hemispheres of a normal adult brain. A. illustrates the hemispheres in Talairach space with overlaid flat map at 50% opacity fit to match the contours of the callosal sulcus (cas). The fine dotted lines circumscribing the dorsal corpus callosum then give the inner boundaries of each cingulate subregion-of-interest (SOI) on the MRI. The inward-pointing long arrows (and one short outward-pointing arrow) mark the rostro–caudal inter-SOI borders on the MRI. But the two outer sets of fine dotted lines on the flat map do not necessarily correspond to any MRI sulcal lines or SOI boundaries. The outer sulcal limits (boundaries) of each SOI must be drawn on the MRI as described in the text. In B., the flat map has been removed to show how the six major SOIs have been drawn according to the method of the text in these two hemispheres with inter- and outer-SOI boundaries now marked by large blue (left) or red (right) dots. C. shows the outer sulcal limits in native, rather than Talairach space. Note the gyral distortions induced by the Talairach transform, including removing part of the paracingulate sulcus (pcgs; circle in B.) The short arrows indicate the dorsal and ventral extrema of the marginal ramus (mr). The splenial sulcus (spls) in PCC and cingulate sulcus (cgs) in ACC are also labeled. The eight cingulate SOIs are: 1, subgenual anterior cingulate cortex (sACC); 2, pregenual anterior cingulate cortex (pACC); 3, anterior midcingulate cortex (aMCC); 4, posterior midcingulate cortex (pMCC); 5, dorsal posterior cingulate cortex (dPCC); 6, ventral posterior cingulate cortex (vPCC); 7, dorsal retrosplenial cortex (dRSC); and 8, ventral retrosplenial cortex (vRSC). Note that, given the limited spatial resolution of the MRI, we have opted not to volume the small dRSC and vRSC SOIs explicitly, but have incorporated them into the dPCC and vPCC, respectively.

TABLE 36.1 Algorithm for parcellating subregions-of-interest (SOIs) in the cingulate gyrus according to the Eight-Subregion Model in Talairach or ICBM152 space

Steps	
	Transformation into atlas space
1	Align MRI whole-brain volume along AC–PC line
2	Transform MRI volume into Talairach or ICBM152 atlas space
	Assigning inter-SOI boundaries and SOI inner boundaries
3	Select a cerebral hemisphere to process
4	In sagittal view, locate midline slice of the hemisphere
5	Scroll to a sagittal slice ~5mm lateral to midline
6	Take a screenshot as jpeg or other graphic format of the slice
7	Import the screenshot into Adobe Photoshop or similar program
8	Download the flat map for subject GPC from www.cingulumneurosciences.org
9	Import the flat map into Photoshop
10	Overlap the flat map at 50% opacity with the MRI
11	Shift, rotate, and resize the flat map to fit the corpus callosum of the MRI
12	Draw the inter-SOI boundaries from the flat map on the MRI
13	Draw the SOI inner boundaries from the flat map on the MRI
	Assigning SOI outer boundaries
14	Identify the pcgs on the sagittal MRI (may entail locating and connecting multiple vertical and horizontal segments)
15	Draw the pcgs as the outer boundary of sACC, pACC, and aMCC
16	Use the cgs as the outer boundary of pMCC, dPCC, and vPCC
	Voluming the SOIs
17	On the MRI, copy the SOI boundaries onto more medial and lateral slices
18	Adjust the boundaries on each slice
19	Continue outlining the SOIs in sagittal view until the sulcal fundi are reached (may occur at different slices for different sulci, within and between SOIs)
20	Sum the enclosed areas across slices and multiply by slice thickness for SOI volumes
21	Repeat for the other hemisphere

SOI, subregion-of-interest; sACC, subgenual anterior cingulate cortex; pACC, pregenual anterior cingulate cortex; aMCC, anterior midcingulate cortex; pMCC, posterior midcingulate cortex; dPCC, dorsal posterior cingulate cortex; vPCC, ventral posterior cingulate cortex.

The parcellations were similar in Talairach space. The volumes measured for these hemispheres in the two spaces are listed in Table 36.2. Note that these are gyral volumes that have not been tissue-segmented into gray matter, white matter, and CSF, though this is a possible addition to the method. For ICBM152, the case-to-case standard deviations of the SOI volumes ranged from 9.4 to 25.7% of the mean; for Talairach, their range was 7.6–23.5%. Some such variation is appropriate considering that the brains have been normalized into a common space. Within cases, SOI volumes differed 1.2–39.7% between the two spaces with the Talairach volumes typically being smaller.

Perspectives on the Cingulate SOI Voluming Method

Co-registering a flat map to sagittal MRI provides a convenient method of linking a wide range of neurobiological observations in a common coordinate system. Although it is true that the macromorphology of cingulate cortex experiences a high degree of variation, much of this variability is overlooked in the framework of a subregional analysis. Setting the outer limits of the ACC and PCC remains a problem in neuron-free structural images but this problem can be standardized across cases. The measurements provided in a small sample above

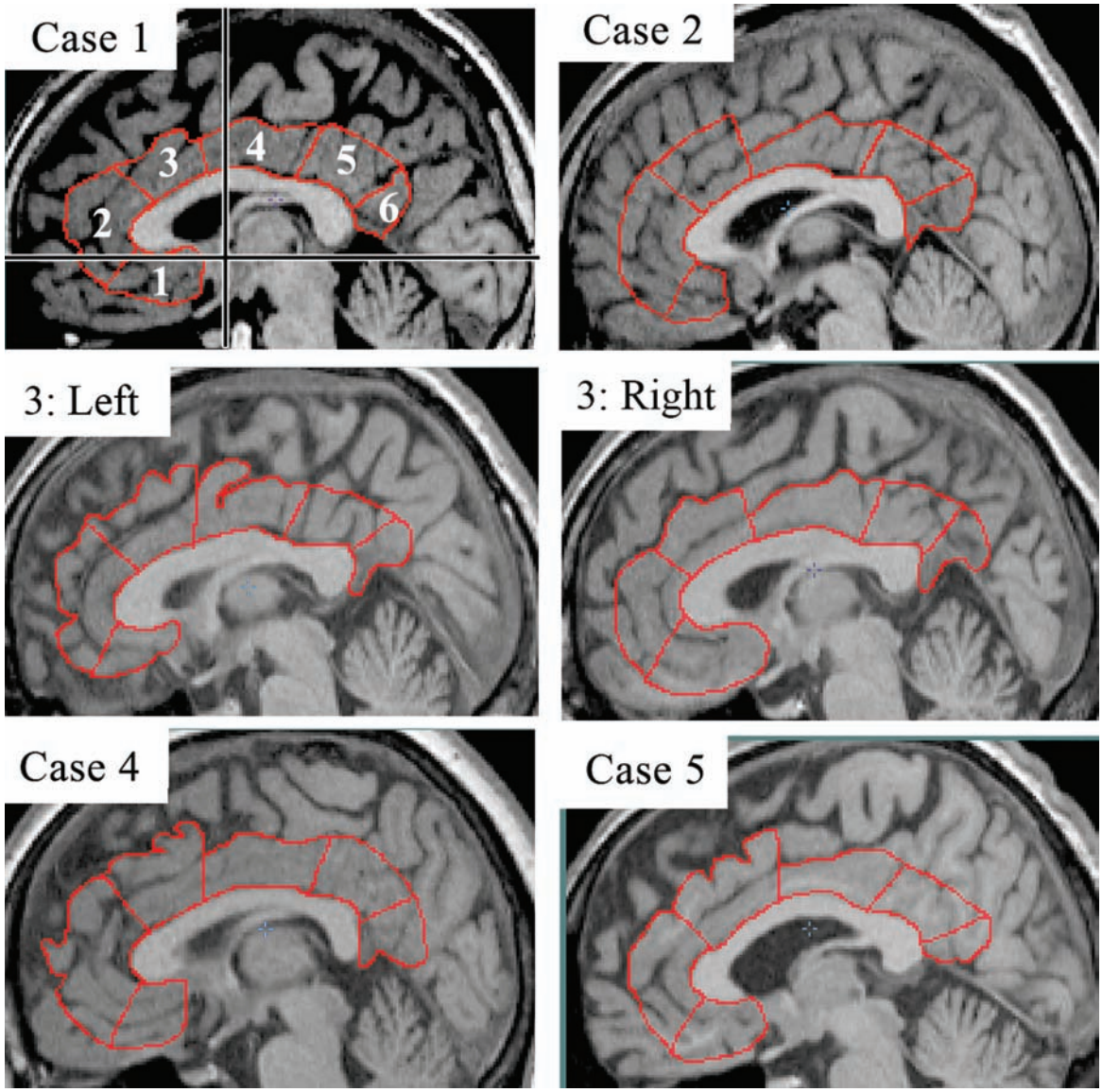

Fig. 36.7 T1-weighted whole-brain MRI transformed into ICBM152 for six normal adult hemispheres. Sections are taken ~5 mm lateral to the sagittal midline. In Case 1, the black horizontal represents the AC–PC line and the black vertical represents the VCA. The red outline indicates the parcellation of the cingulate gyrus into subregions-of-interest (SOIs) according to the method of the text. 1, subgenual anterior cingulate cortex (sACC); 2, pregenual anterior cingulate cortex (pACC); 3, anterior midcingulate cortex (aMCC); 4, posterior midcingulate cortex (pMCC); 5, dorsal posterior cingulate cortex (dPCC); and 6, ventral posterior cingulate cortex (vPCC). The two remaining cingulate SOIs of the Eight-Subregion Model—the dorsal retrosplenial cortex (dRSC) and the ventral retrosplenial cortex (vRSC)—have been included in the dPCC and vPCC, respectively. Results were similar for Talairach & Tournoux space.

suggest that differences between the Talairach and ICBM152 coordinate systems is modest and greater comparability of findings may be possible with a consistent use of this method.

Reservations are appropriate as the technique has been tested on only six cerebral hemispheres from a sample of five subjects. This clearly falls far from exhausting the range of cingulate macroanatomy and also may be atypical. The SOI assignments were not verified histologically in our human *in vivo* sample, although we did use the histologically verified *post-mortem* case GPC to create them. We used only one histologically verified case, although past studies with series of 6–8 cases (Vogt *et al.*, 2003, 2006) showed little intersubject variation in the inter-SOI boundaries and the mean boundaries from the VCA were closely

TABLE 36.2 Volumes (mm^3) of six cingulate subregions-of-interest in six hemispheres of five healthy adult subjects

Case	Sex	Age, year	Hemisphere	SOI	Talairach	ICBM152
1	M	38	R	sACC	3,323	3,605
				pACC	5,909	6,484
				aMCC	3,383	3,719
				pMCC	3,748	4,748
				dPCC	4,769	4,954
				vPCC	2,379	2,451
2	M	27	R	sACC	3,313	3,273
				pACC	7,173	6,751
				aMCC	5,238	5,128
				pMCC	3,680	4,969
				dPCC	5,261	4,570
				vPCC	2,791	3,129
3	M	48	L	sACC	2,960	2,885
				pACC	6,753	7,052
				aMCC	4,817	5,808
				pMCC	5,525	5,234
				dPCC	3,876	4,592
				vPCC	2,926	3,138
3	M	48	R	sACC	3,303	4,939
				pACC	5,881	6,083
				aMCC	4,088	5,292
				pMCC	3,491	4,116
				dPCC	5,161	4,134
				vPCC	2,505	2,260
4	F	22	L	sACC	2,804	2,926
				pACC	7,012	9,360
				aMCC	4,909	6,547
				pMCC	3,909	5,048
				dPCC	5,277	5,257
				vPCC	3,659	3,875
5	F	44	L	sACC	2,907	2,498
				pACC	5,878	5,449
				aMCC	3,538	5,814
				pMCC	2,789	3,561
				dPCC	4,562	4,183
				vPCC	3,111	2,227
Means±SD		35.8±11.0		sACC	3,102±237	3,354 ± 862
				pACC	6,434±612	6,863 ± 1,344
				aMCC	4,329±772	5,385 ± 955
				pMCC	3,857±906	4,613± 644
				dPCC	4,818±544	4,615±435
				vPCC	2,895±460	2,847±649

correlated to this subject. Moreover, a large amount of variation in native space is removed once the flat map had been put into Talairach space and co-registered to all other subjects.

The method requires acquisition of high-resolution structural MRI (1.5 T field strength is sufficient, 3 T would arguably be better), but such scans are increasingly routine in clinic and research. The RSC and its dRSC and vRSC SOIs were not delineated separately but rather incorporated into the dPCC and vPCC. Separate delineations of these two SOIs may be more readily achieved with other techniques including higher-resolution MRI. Additionally, the method assumes that the inter-SOI rostral-caudal boundaries do not change along the medial–lateral dimension, which need not be the case. Overall, the method yields a comprehensive and unambiguous parcellation of the cingulate cortex attained at reasonable cost in time and effort and offering precision sufficient for most neuroimaging studies of the cingulate cortex as currently practiced.

Acknowledgments

The authors gratefully acknowledge Drs James R. MacFall and Martha E. Payne of the Neuropsychiatric Imaging Research Laboratory (NIRL) of Duke University Medical Center for collaborative assistance and training and support of one of us (TS). This work was partly funded by grants R03DA20512-01 and R21DA023192-01 from the National Institute on Drug Abuse (NIDA) to JON. For the generous support, the authors also wish to thank the Brain Mapping Medical Research Organization, Brain Mapping Support Foundation, Pierson-Lovelace Foundation, Ahmanson Foundation, Tamkin Foundation, Jennifer Jones-Simon Foundation, Capital Group Companies Charitable Foundation, Robson Family, William M. and Linda R. Dietel Philanthropic Fund at the Northern Piedmont Community Foundation, Northstar Fund, and the National Center for Research Resources grants RR12169, RR13642, and RR08655.

References

Blanton, R. E., Levitt J. G., Thompson, P. M., Narr, K. L., Capetillo-Cunliffe, L., Nobel, A., Singerman, J. D., McCracken, J. T, & Toga A. W. (2001) Mapping cortical asymmetry and complexity patterns in normal children. *Psychiatry Res Neuroimag 107*: 29–43.

Brodmann, K. (1909). Vergleichende Lokalisationslehre der Grosshirnrinde in ihren Prinzipien dargestellt auf Grund des Zellenbaues. Leipzig: Barth.

Collins, D. L. (1994) PhD thesis, McGill University.

Evans, A. C., Collins, D. L., Miulls, S. R., Brown, E. D., Kelly R. L., & Peters T. M. (1993) 3D statistical neuroanatomical models from 305 MRI volumes. *Proc IEEE-Nucl Sci Symp Med Imaging Conf* 1813–1817.

Mazziotta, J. C., Toga, A. W., Evans, A., Fox, P., & Lancaster, J. (1995) A probabilistic atlas of the human brain: theory and rationale for its development. *NeuroImage 2*: 89–101.

McCormick, L. M., Ziebell, S., Nopoulos, P., Cassell, M., Andreasen, N. C., & Brumm, M. (2006) Anterior cingulate cortex: an MRI-based parcellation method. *NeuroImage 32*: 1167–1175.

Shattuck, D. W., Sandor-Leahy, S. R., Schaper, K. A., Rottenberg, D. A., & Leahy, R. M. (2001). Magnetic resonance image tissue classification using a partial volume model. *NeuroImage 13*: 856–876.

Sikes, R. W., Vogt, L. J., & Vogt, B. V. (2008) Distribution and properties of visceral nociceptive neurons in rabbit cingulate cortex. *Pain 135*: 160–174.

Talairach, J., & Szikla, G. (1967) *Atlas d'anatomie stereotaxique du telencephale: etudes anatomo-radiologiques*. Paris: Masson et Cie.

Talairach, J., & Tournoux, P. (1988). *Co-planar Stereotaxic Atlas of the Human Brain*. NY: Thieme Medical Publishers.

Vogt, B. A. (1993) Structural organization of cingulate cortex: Areas, neurons, and somatodendritic transmitter receptors. In B. A. Vogt, & M. Gabriel (Eds), *Neurobiology of Cingulate Cortex and Limbic Thalamus*. (pp. 19–70). Boston: Birkhäuser Boston, Inc.

Vogt, B. A., Berger, G. R., & Derbyshire, S. W. G. (2003) Structural and functional dichotomy of human midcingulate cortex. *Eur J Neurosci 18*: 3134–3144.

Vogt, B. A., Hof, P. R., & Vogt, L. J. (2004b) Cingulate gyrus. In G. Paxinos & J. Mai (Eds), *The Human Nervous System* (2nd edn), Chapter 24 (pp. 915–950).

Vogt, B. A., Vogt, L., & Laureys, S. (2006) Cytology and functionally correlated circuits of human posterior cingulate areas. *NeuroImage 29*: 452–466.

Vogt, B. A., Vogt, L. J., & Farber, N. B. (2004a) Cingulate cortex and disease models. In G. Paxinos (Ed.), *The Rat Nervous System* (3rd Edn). (pp. 705–727). SanDiego: Elsevier.

Vogt, B. A., Vogt, L. J., Farber, N. B., & Bush, G. (2005) Architecture and neurocytology of monkey cingulate cortex. *J Comp Neurol 485*: 218–239.

Vogt, B. A., Vogt, L. J., Perl, D. P., & Hof, P. R. (2001) Cytology of human caudomedial cingulate, retrosplenial, and caudal parahippocampal cortices. *J Comp Neurol 438*: 353–376.

Zilles, K., & Palomero-Gallagher, N. (2001) Cyto-, myelo-, and receptorarchitectonics of the human parietal cortex. *NeuroImage 14*: 8–20.